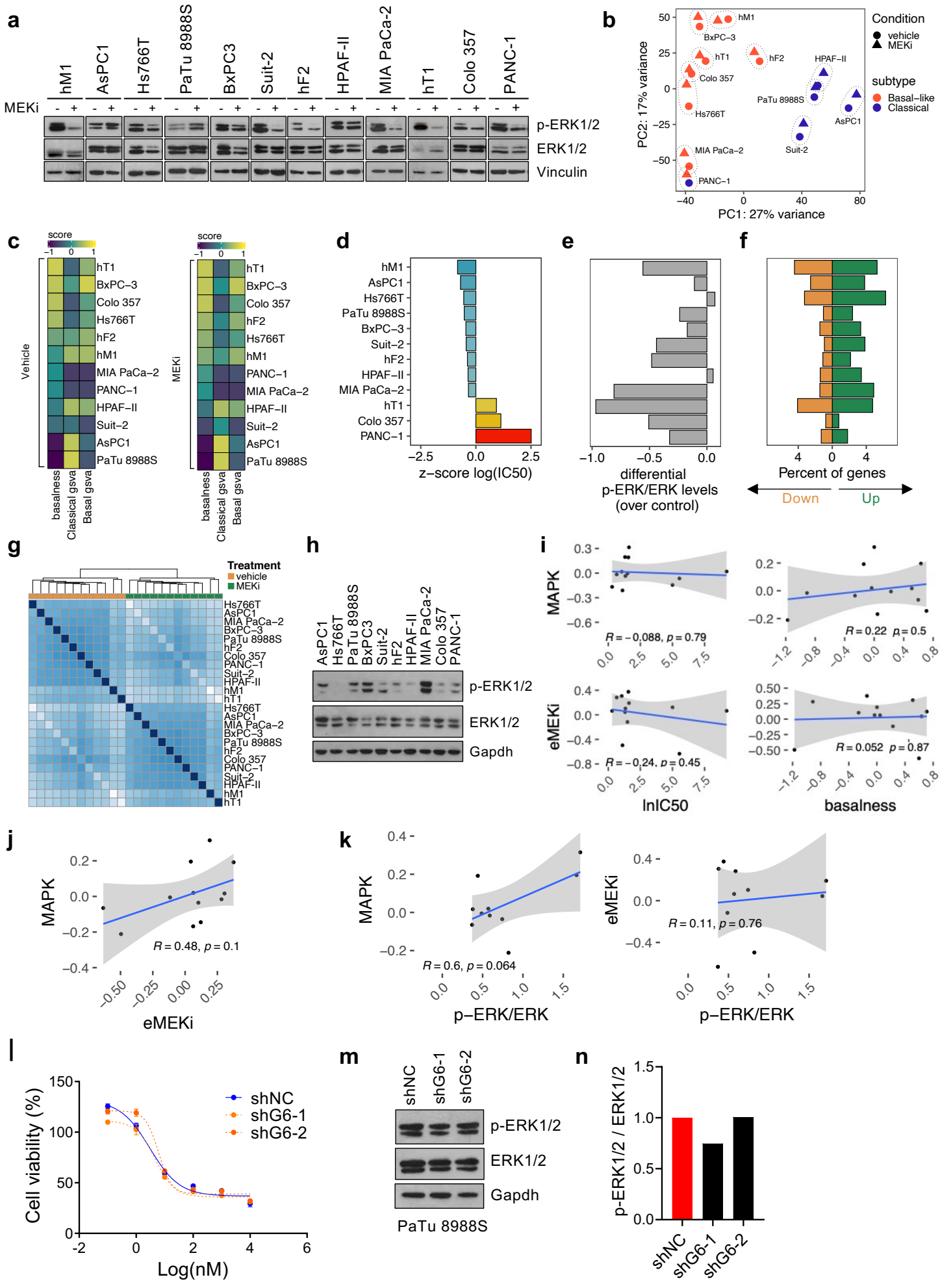
a
hM1
AsPC1
Hs766T
PaTu 8988S
BxPC3
Suit-2
hF2
HPAF-II
MIA PaCa-2
hT1
Colo 357
PANC-1
MEKi
p-ERK1/2
ERK1/2
Vinculin
b
Condition
vehicle
MEKi
subtype
Basal-like
Classical
PC2: 17% variance
PC1: 27% variance
c
score
Vehicle
MEKi
basalness
Classical gsva
Basal gsva
d
z-score log(IC50)
e
differential
p-ERK/ERK levels
(over control)
f
Percent of genes
Down
Up
g
Treatment
vehicle
MEKi
h
p-ERK1/2
ERK1/2
Gapdh
i
MAPK
eMEKi
lnIC50
basalness
R = −0.088, p = 0.79
R = 0.22 p = 0.5
R = −0.24, p = 0.45
R = 0.052 p = 0.87
j
MAPK
eMEKi
R = 0.48, p = 0.1
k
MAPK
eMEKi
p−ERK/ERK
R = 0.6, p = 0.064
R = 0.11, p = 0.76
l
Cell viability (%)
Log(nM)
shNC
shG6-1
shG6-2
m
shNC
shG6-1
shG6-2
p-ERK1/2
ERK1/2
Gapdh
PaTu 8988S
n
p-ERK1/2 / ERK1/2

Supplementary Figure 1: Short-term MEK inhibition does not affect PDAC epithelial subtype. a Immunoblot of phospho-ERK1/2 and total ERK1/2 in whole cell lysates of 12 human PDAC cell lines after 48 hours of MEKi treatment with sub-IC50 doses. Vinculin, loading control. **b** Principal Component Analysis (PCA) of RNA-seq data from 12 human cell lines treated with vehicle or MEKi for 2 days, classified as classical or basal-like according to Moffitt's subtypes[1]. **c** Heatmaps displaying the individual GSVA score for basal-like and classical signatures, and the "basalness" score (computed as subtraction of the GSVA_Moffitt_Classical_score to the GSVA_Moffitt_Basal_score). **d** Barplot showing the z-score (Log IC50) for MEKi sensitivity of 12 human PDAC cell lines ordered top-to-bottom from the most sensitive to the least sensitive. **e** Barplot showing the differential phospho-ERK levels following MEKi (from panel a, Source data are provided as Source Data file). **f** Barplot showing the percentage of up- and down-regulated genes in 12 PDAC cell lines treated with MEKi for 2 days. **g** Heatmap illustrating transcriptional similarity between cell lines after batch correction, showing transcriptional changes induced by MEKi. **h** Immunoblot of phospho-ERK1/2 and total ERK1/2 in whole cell lysates of human PDAC cell lines. GAPDH, loading control. **i** Scatter plots showing correlation between MAPK transcriptional signatures and "basalness" or MEKi sensitivity (lnIC50) for 12 human cancer cell lines. p value from *r* correlation test. Grey area represents 95% (CI) . **j** Scatter plot showing the correlation between the two MAPK transcriptional signatures. p value from *r* correlation test. Grey area represents 95% CI. **k** Scatter plots showing the correlation between MAPK transcriptional signatures and basal p-ERK levels in 10 human cancer cell lines. p value from *r* correlation test. Grey area represents 95% CI. **l** MEKi dose-response curve for a 3-day cell-titer-glo assay with PaTu 8988S transduced with mock (shNC) or GATA6-targeting shRNAs (shG6-1, shG6-2). **m** Immunoblot of phospho-ERK1/2 and total ERK1/2 in whole cell lysates of PaTu 8988S transduced with mock (shNC) or shRNAs targeting GATA6 (shG6-1, shG6-2). **n** Barplot showing the quantification of relative phopho-ERK1/2 level shown in Supplementary Fig. 1m. n = 2 biological replicates.

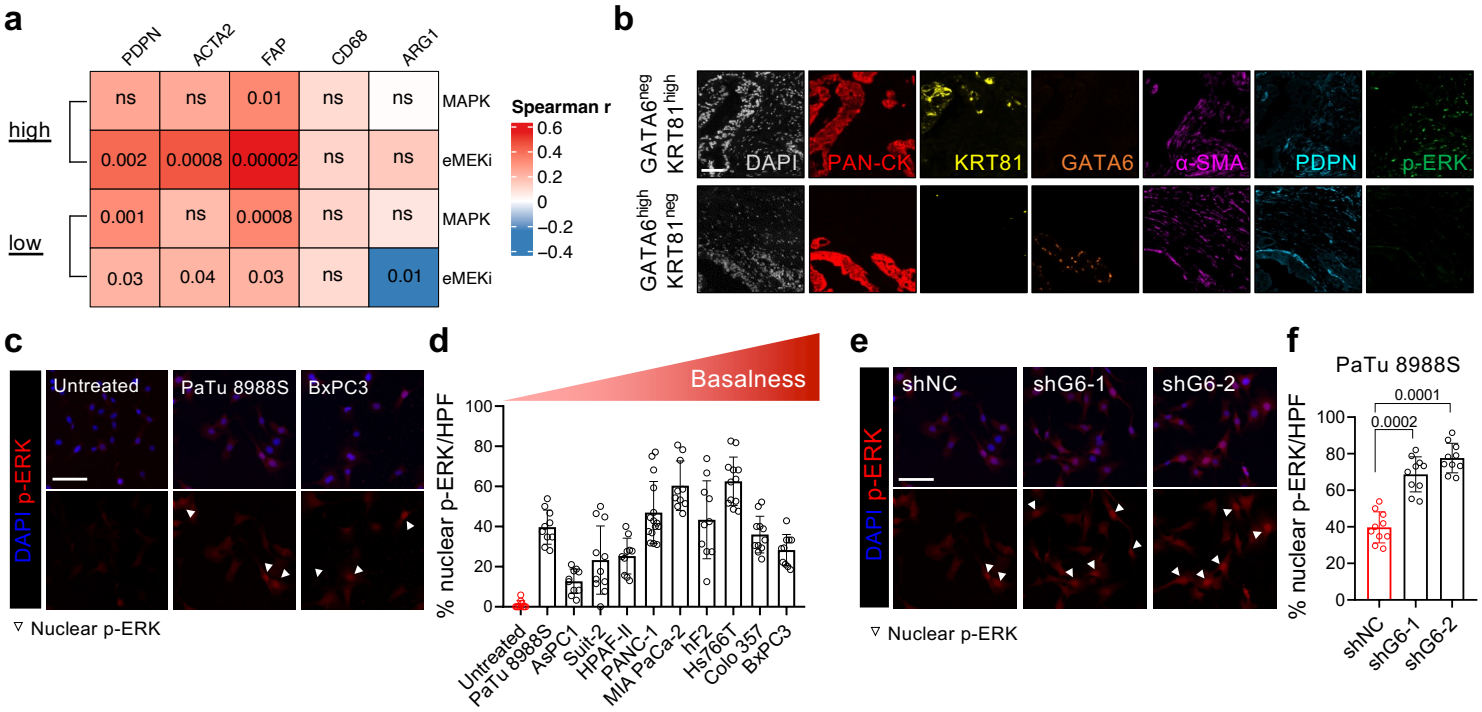

Supplementary Figure 2: p-ERK⁺ fibroblasts are associated with basal-like cancer cells. a Heatmap showing Spearman's correlation between gene signatures and selected markers for fibroblasts and macrophages in samples from the TCGA cohort[2], stratified by neoplastic cell content (high > 40%). **b** Representative areas from Fig. 1b showing individual fluorescence channels. Scale bar, 100 µm. **c** Representative Immunofluorescence staining of p-ERK1/2 on mPSCs FBS-starved for 6 hours (untreated) and treated for 10 minutes with conditioned media from cell lines with different "basalness" levels. Nuclei were counterstained with DAPI (blue). Scale bar, 100 µm. **d** Scatter dot plot showing the percentage of cells with nuclear p-ERK per field of visualization (FOV; n ≥ 10/condition). Results presented as mean values ± S.D. **e** Representative Immunofluorescence staining of p-ERK on mPSCs (as in c) treated with conditioned media from PaTu 8988S transduced with either mock (shNC) or shRNAs targeting GATA6 (shG6-1, shG6-2). Scale bar, 100 µm. **f** Scatter dot plot showing nuclear p-ERK quantification. p values determined by Mann Whitney test (two-sided). PaTu 8988S transduced with shNC was used as baseline in Supplementary Fig. 2 c, d . (n ≥ 10 FOV /condition). Results presented as mean values ± S.D.

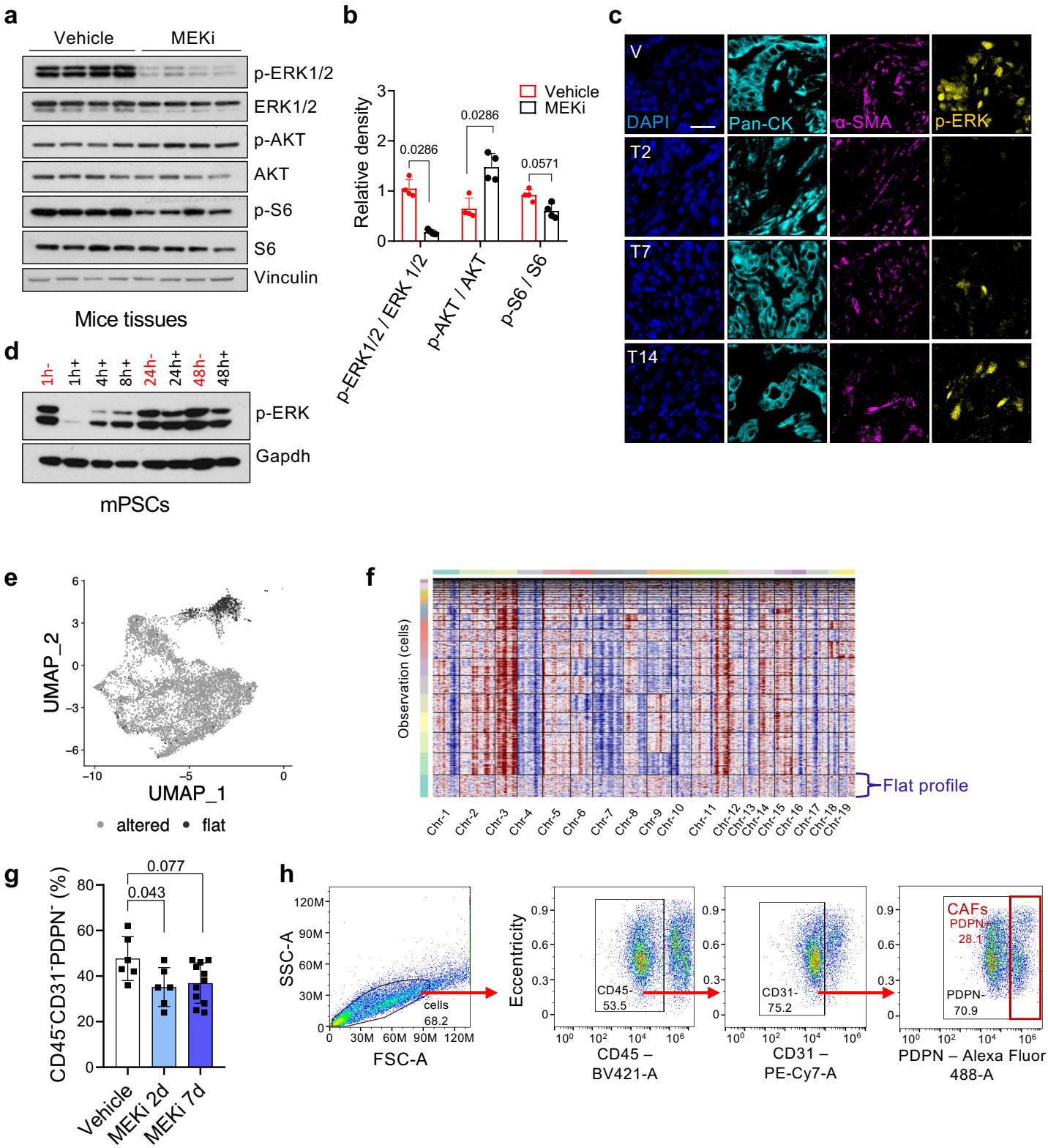
a
Vehicle
MEKi
p-ERK1/2
ERK1/2
p-AKT
AKT
p-S6
S6
Vinculin
Mice tissues
b
Relative density
Vehicle
MEKi
0.0286
0.0286
0.0571
p-ERK1/2 / ERK 1/2
p-AKT / AKT
p-S6 / S6
c
V
DAPI
Pan-CK
α-SMA
p-ERK
T2
T7
T14
d
1h-
1h+
4h+
8h+
24h-
24h+
48h-
48h+
p-ERK
Gapdh
mPSCs
e
UMAP_2
UMAP_1
altered
flat
f
Observation (cells)
Flat profile
Chr-1
Chr-2
Chr-3
Chr-4
Chr-5
Chr-6
Chr-7
Chr-8
Chr-9
Chr-10
Chr-11
Chr-12
Chr-13
Chr-14
Chr-15
Chr-16
Chr-17
Chr-18
Chr-19
g
CD45-CD31-PDPN- (%)
0.077
0.043
Vehicle
MEKi 2d
MEKi 7d
h
SSC-A
FSC-A
cells
68.2
Eccentricity
CD45-
53.5
CD31-
75.2
CAFs
PDPN+
28.1
PDPN-
70.9
CD45 –
BV421-A
CD31 –
PE-Cy7-A
PDPN – Alexa Fluor
488-A

Supplementary Figure 3: MEK inhibition is efficient at 2 days of treatment and increases the stroma content *in vivo.* **a** Immunoblot of p-ERK1/2, total ERK1/2, p-AKT, total AKT, p-S6, and total S6 in whole-tumour lysate from mice treated for 2 days either with vehicle (n = 4 mice) or MEK inhibitor 1 mg/kg (n = 4 mice). Vinculin was used as loading control. **b** Scatter dot plot showing the quantification of changes in the phosphorylated levels of proteins (p-ERK1/2, p-AKT, and p-S6) shown in Supplementary Fig. 3a. p values as determined by Mann Whitney test (two-sided). n = 4 mice/ condition. Results presented as mean values ± S.D. **c** Representative areas from Fig. 2b displaying individual fluorescence channels for mice treated with vehicle (C), MEKi for 2 (T2), 7 (T7), and 14 (T14) days. Scale bar, 25 µm. **d** Immunoblot of p-ERK1/2 in whole-cell lysate from mPSCs treated with either vehicle (red) or MEKi at different timepoints. GAPDH was used as loading control. **e** UMAP plot showing cells from the epithelial cluster coloured according to copy number profile (grey, altered; black, flat). **f** Representative heatmap showing inferred amplifications (red) and deletions (blue) for the sample T7 (mice treated for 7 days with MEKi) from transcriptomic data for each cell (rows) over the genomic positions (columns). Horizontal black line show cells hierarchical clustering based on CNV profile. **g** FACS analysis of tumour tissues from tumour-bearing mice treated with MEKi for 2 or 7 days. The barplots show the percentage of live cells calculated on the total of immune ($CD45^+$) and stromal ($CD31^+$ and $PDPN^+$) cells. n ≥ 6 mice/condition. Results presented as mean values ± S.D. **h** Flow plots showing the gating strategy used in Fig. 2i and Supplementary Fig. 2g.

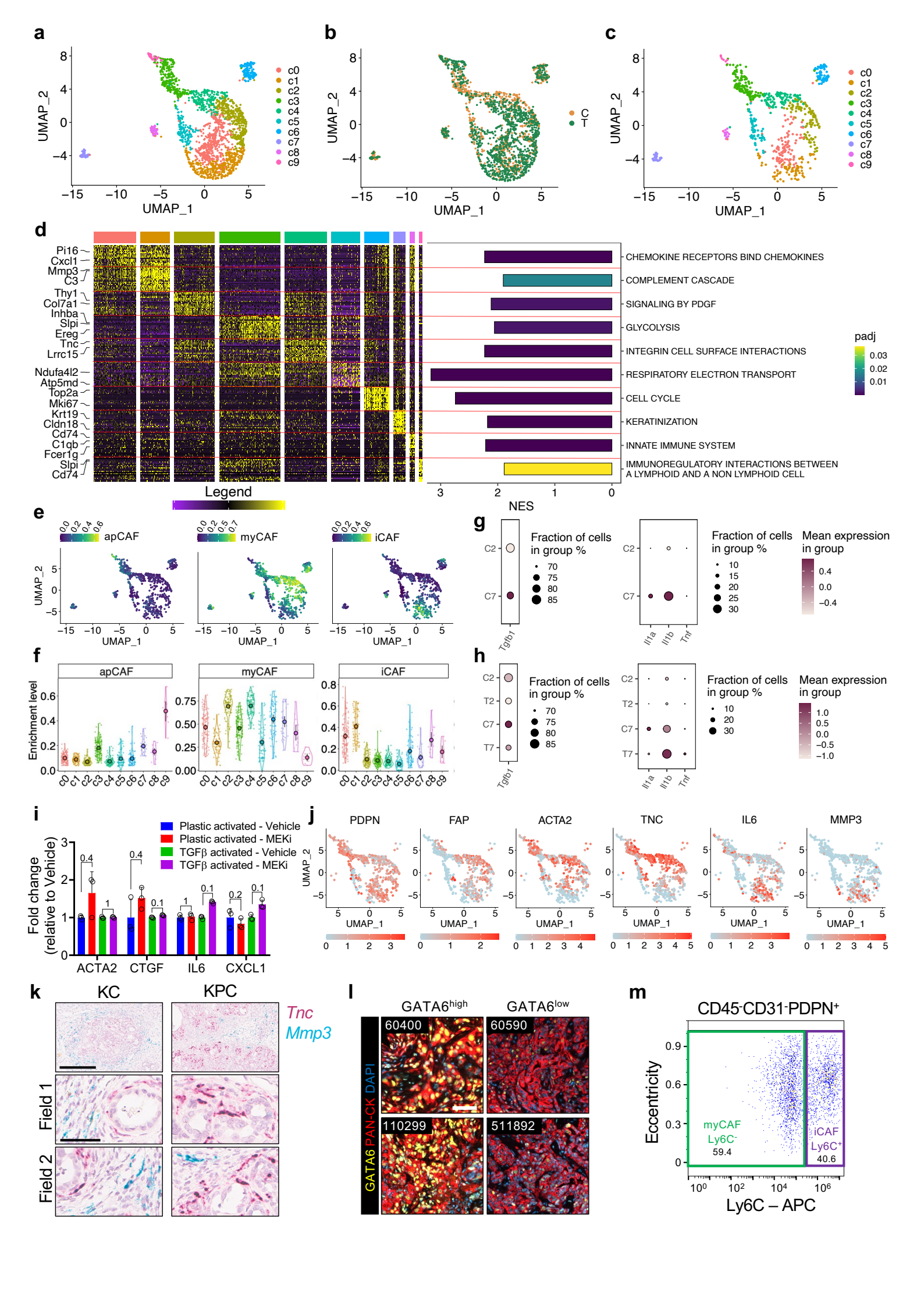
a
b
c
UMAP_1
UMAP_2
c0
c1
c2
c3
c4
c5
c6
c7
c8
c9
C
T
d
Pi16
Cxcl1
Mmp3
C3
Thy1
Col7a1
Inhba
Slpi
Ereg
Tnc
Lrrc15
Ndufa4l2
Atp5md
Top2a
Mki67
Krt19
Cldn18
Cd74
C1qb
Fcer1g
Slpi
Cd74
CHEMOKINE RECEPTORS BIND CHEMOKINES
COMPLEMENT CASCADE
SIGNALING BY PDGF
GLYCOLYSIS
INTEGRIN CELL SURFACE INTERACTIONS
RESPIRATORY ELECTRON TRANSPORT
CELL CYCLE
KERATINIZATION
INNATE IMMUNE SYSTEM
IMMUNOREGULATORY INTERACTIONS BETWEEN A LYMPHOID AND A NON LYMPHOID CELL
padj
0.03
0.02
0.01
Legend
NES
e
apCAF
myCAF
iCAF
f
Enrichment level
g
h
Fraction of cells in group %
Mean expression in group
Tgfb1
Il1a
Il1b
Tnf
i
Plastic activated - Vehicle
Plastic activated - MEKi
TGFβ activated - Vehicle
TGFβ activated - MEKi
Fold change (relative to Vehicle)
ACTA2
CTGF
IL6
CXCL1
j
PDPN
FAP
ACTA2
TNC
IL6
MMP3
k
KC
KPC
Tnc
Mmp3
Field 1
Field 2
l
GATA6high
GATA6low
60400
60590
110299
511892
GATA6 PAN-CK DAPI
m
CD45-CD31-PDPN+
Eccentricity
myCAF
Ly6C-
59.4
iCAF
Ly6C+
40.6
Ly6C – APC

Supplementary Figure 4: MEKi result into increased iCAFs frequency in mouse PDAC. a UMAP plot of fibroblast subclusters, colour-coded by cell type. **b** UMAP plot of cells from the fibroblast cluster of integrated samples of vehicle- and MEKi-treated mice **c** UMAP plot of fibroblasts from untreated tumour-bearing mice, colour-coded as in a. **d** Heatmap showing the relative average expression of the most enriched genes for each cluster, showing two representative genes per cluster together with pathway enrichment analysis using GSEA[3]. See Supplementary Data 3. **e** Feature plot showing enrichment of mouse apCAF, myCAF, and iCAF signatures[4] in the scRNA-seq dataset. **f** Violin plots showing enrichment of the Elyada's signatures[4] in the clusters from c. Data are presented as mean values and 95% CI. **g** Dot plot of scaled average expression of selected genes in malignant cells from tumour-bearing mice at different progression stages (C2 vs C7). Colour intensity shows expression level; dot size shows the percentage of expressing cells. **h** Dot plot of scaled average expression of selected genes in malignant cells from tumour-bearing mice treated with MEKi for 2 (T2) or 7 (T7) days vs. matched controls (C2, C7). Colour intensity represents expression level, dot size represent the percentage of expressing cells. **i** MEKi treatment induced changes in mRNA expression of myCAF (*Acta2, Ctgf*) and iCAF (*Il6, Cxcl1*) markers in mouse PSCs activated by either plastic cultivation or TGF-β1. p values determined by Mann Whitney test (two-sided). n = 3 technical replicates. Results presented as mean values ± S.D. **j** UMAP plot showing normalized expression of selected markers (*Pdpn, Fap, Acta2, Il6, Tnc,* and *Mmp3*) in fibroblast cluster cells from vehicle-treated mice. **k** Representative *in situ* hybridization images showing expression of *Tnc* (myCAFs) and *Mmp3* (iCAFs) in tissues from KC and KPC mice. Scale bar, 300 µm (main), 60 µm (insets). **l** Representative multiplex immunofluorescence images of murine PDAC tissues from orthotopic transplantation of classical or basal-like murine cell lines. Scale bar, 50 µm. **m** Flow plots showing the gating strategy to distinguish myCAFs from iCAFs. See also Fig. 3h.

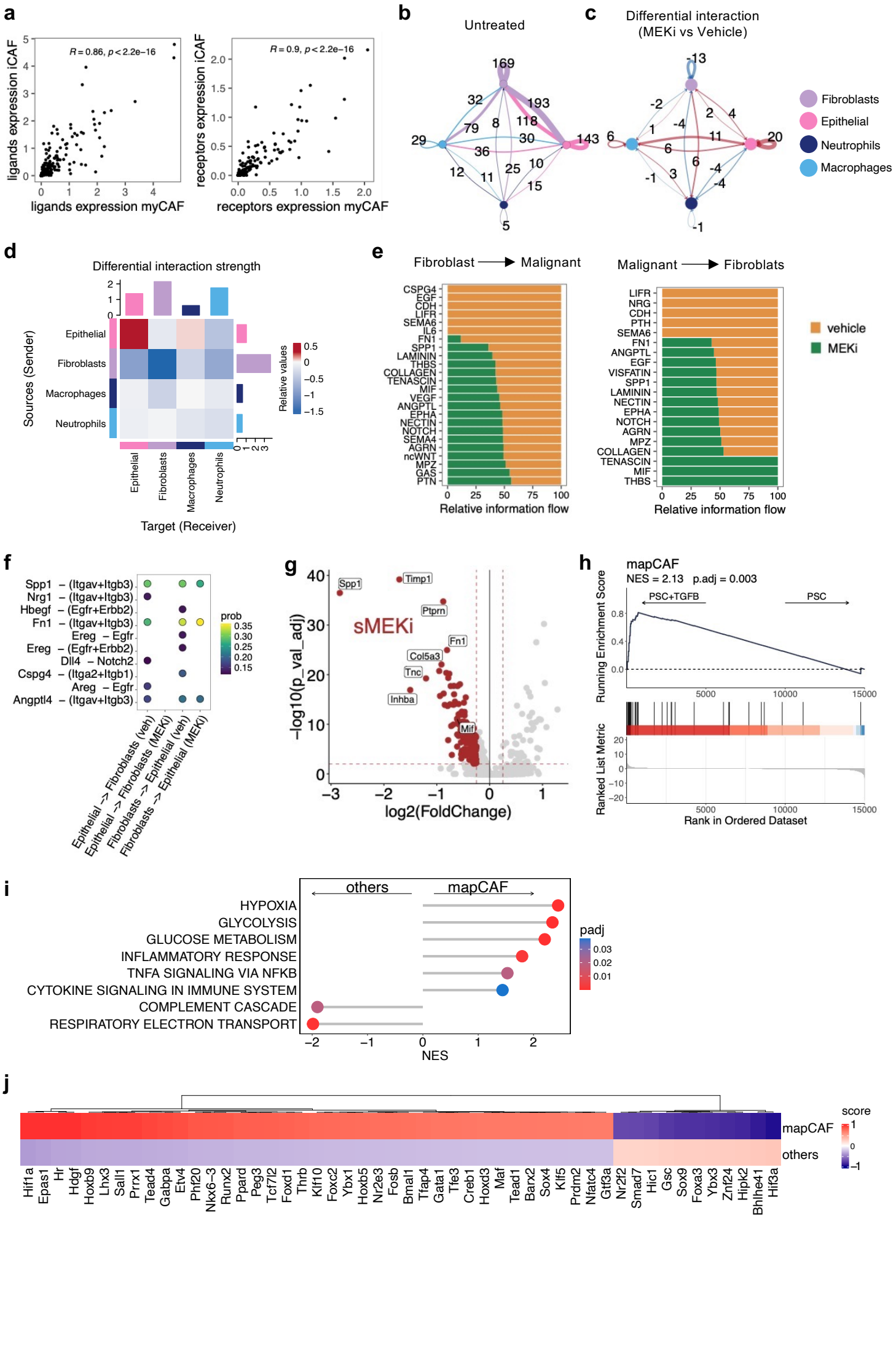
a
ligands expression iCAF
ligands expression myCAF
R = 0.86, p < 2.2e−16
receptors expression iCAF
receptors expression myCAF
R = 0.9, p < 2.2e−16
b
Untreated
c
Differential interaction
(MEKi vs Vehicle)
Fibroblasts
Epithelial
Neutrophils
Macrophages
d
Differential interaction strength
Sources (Sender)
Target (Receiver)
Epithelial
Fibroblasts
Macrophages
Neutrophils
Relative values
e
Fibroblast → Malignant
Malignant → Fibroblats
Relative information flow
vehicle
MEKi
f
Spp1 – (Itgav+Itgb3)
Nrg1 – (Itgav+Itgb3)
Hbegf – (Egfr+Erbb2)
Fn1 – (Itgav+Itgb3)
Ereg – Egfr
Ereg – (Egfr+Erbb2)
Dll4 – Notch2
Cspg4 – (Itga2+Itgb1)
Areg – Egfr
Angptl4 – (Itgav+Itgb3)
prob
Epithelial -> Fibroblasts (veh)
Epithelial -> Fibroblasts (MEKi)
Epithelial -> Epithelial (veh)
Fibroblasts -> Epithelial (MEKi)
g
sMEKi
−log10(p_val_adj)
log2(FoldChange)
h
mapCAF
NES = 2.13 p.adj = 0.003
PSC+TGFB
PSC
Running Enrichment Score
Ranked List Metric
Rank in Ordered Dataset
i
others
mapCAF
HYPOXIA
GLYCOLYSIS
GLUCOSE METABOLISM
INFLAMMATORY RESPONSE
TNFA SIGNALING VIA NFKB
CYTOKINE SIGNALING IN IMMUNE SYSTEM
COMPLEMENT CASCADE
RESPIRATORY ELECTRON TRANSPORT
padj
NES
j
mapCAF
others
score

Supplementary Figure 5: Identification of a gene expression signature of CAFs with elevated MAPK activity. a Pearson correlation of ligand and receptor gene expression between major CAF subtypes. **b** Number of inferred interactions between malignant cells, fibroblasts, macrophages, and neutrophils based on CellChat[5] analysis of scRNA-seq data of untreated tumours. **c** Number of differential connections between the selected cell types in MEKi-treated tumours compared to untreated tumours. **d** Differential interaction strengths inferred between the annotated cell type pairs upon MEKi. The overall change in interaction strengths for a given cell type either as receiver or sender is reported in the barplot at the top and right-hand side of the heatmap, respectively. **e** Stacked barplot showing all the statistically significant ($p < 0.05$, paired Wilcoxon test) signalling pathways ranked based on their differences of overall information flow within the inferred networks between treated and untreated tumours. **f** Dot plot showing selected ligand-receptor interactions and their strengths. **g** Volcano plot representing the differentially expressed genes in fibroblasts upon treatment with MEKi for 2 days. The red dots are the genes defining the sMEKi signature (n = 169). Highlighted some of the genes with log2FC expression < -2 and adjusted $p < 0.05$. **h** GSEA plot showing the enrichment of the mapCAF signature in mPSCs treated with 5 ng/mL of TGF-β1 for 72 hours. **i** Enrichment analysis of significantly up- and down-regulated pathways in mapCAFs. **j** Transcription factor activity inference for the indicated cell subsets using decoupleR[6] on scRNA-seq data.

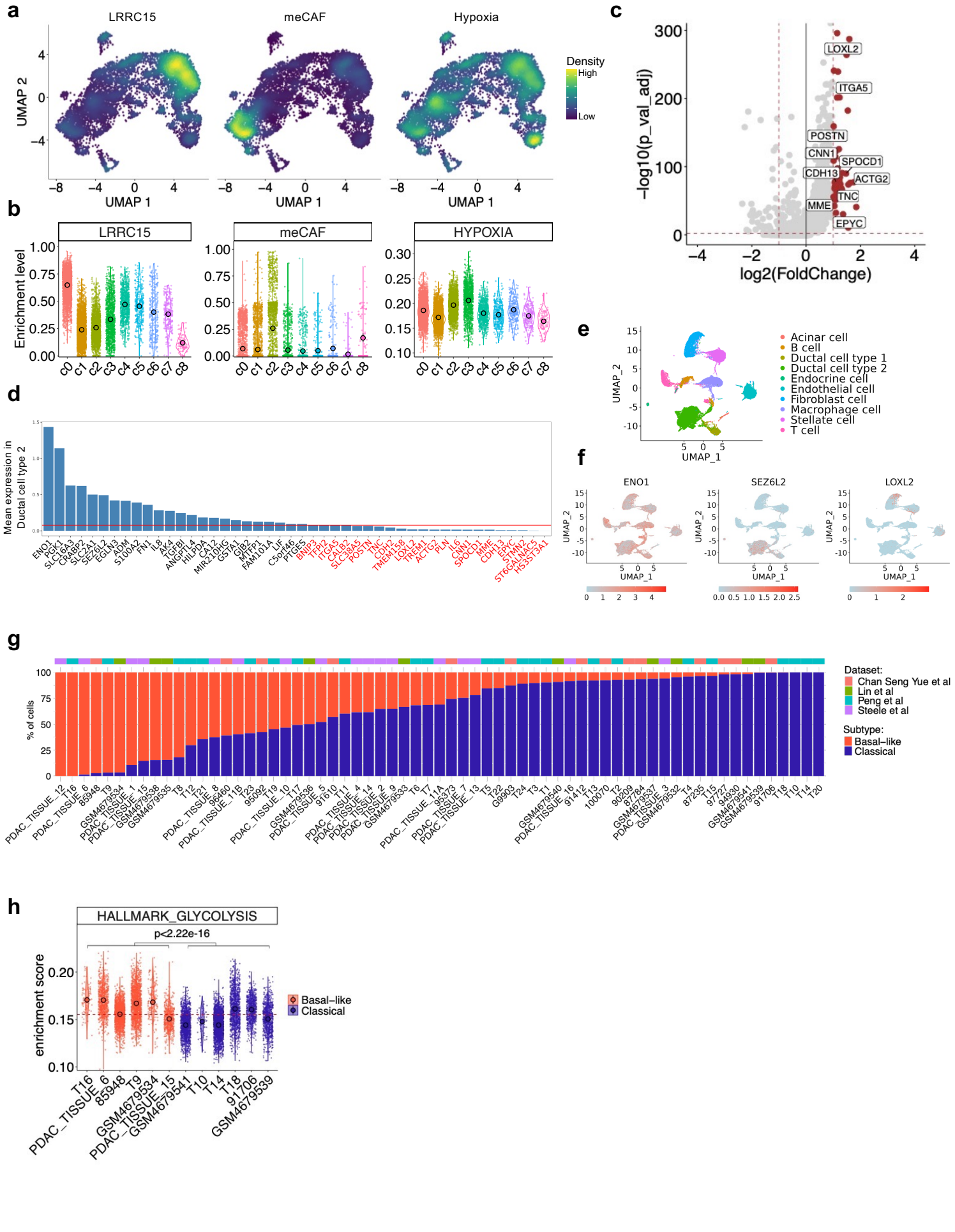
a
LRRC15
meCAF
Hypoxia
UMAP 2
UMAP 1
Density
High
Low
b
LRRC15
meCAF
HYPOXIA
Enrichment level
c0 c1 c2 c3 c4 c5 c6 c7 c8
c
−log10(p_val_adj)
log2(FoldChange)
LOXL2
ITGA5
POSTN
CNN1
SPOCD1
CDH13
ACTG2
TNC
MME
EPYC
d
Mean expression in Ductal cell type 2
ENO1 PGK1 SLC16A3 CRABP2 SLC2A1 SEZ6L2 EGLN3 ADM S100A2 FN1 IL8 AK4 TGFBI ANGPTL4 HILPDA CA12 MIR210HG GSTA1 GIB2 MTFP1 FAM101A UF C5orf46 PTGES BNIP3 TFPI2 ITGA5 CALB2 SLC38A5 POSTN TNC CDH2 TMEM158 LOXL2 TREM1 ACTG2 PLN IL6 CNN1 SPOCD1 MME CDH13 EPYC STMN2 ST6GALNAC5 HS3ST3A1
e
UMAP_2
UMAP_1
Acinar cell
B cell
Ductal cell type 1
Ductal cell type 2
Endocrine cell
Endothelial cell
Fibroblast cell
Macrophage cell
Stellate cell
T cell
f
ENO1
SEZ6L2
LOXL2
g
% of cells
Dataset:
Chan Seng Yue et al
Lin et al
Peng et al
Steele et al
Subtype:
Basal−like
Classical
h
HALLMARK_GLYCOLYSIS
p<2.22e-16
enrichment score
Basal−like
Classical

Supplementary Figure 6: Identification of a human mapCAF signature. a Density plot showing enrichment of human LRRC15[7], meCAFs[8], and the Hypoxia_Hallmark signatures in the human scRNA-seq dataset. **b** Violin plots showing enrichment of the human LRRC15[7], meCAFs[8], and the Hypoxia_Hallmark signatures in the clusters from Fig. 5a. Data are presented as mean values and 95% CI. **c** Volcano plot representing the differentially expressed genes from the comparison between fibroblasts displaying high vs low MAPK transcriptional activity (based on sMEKi levels). The red dots are some of the genes defining the mapCAF signature (n = 22). **d** Average expression of genes of the extended mapCAF signature (n = 46) in the malignant compartment of the scRNA-seq dataset from Peng et al. [9]. Genes included in the final version of the mapCAF signature are coloured in red. **e** UMAP plot showing cell type annotation of the scRNA-seq dataset from Peng et al. [9]. **f** UMAP plots of cells from Peng et al.[9]. coloured by gene expression of the indicated genes. **g** Samples from the harmonized scRNA-seq dataset[9-12] ranked from left to right based on the proportion of basal-like or classical cells. **h** Scatter plots showing the enrichment of the Hallmark_Glycolysis signature in the malignant compartment of PDAC cases with prevalence of basal-like cells from g. p values as determined by Wilcoxon after aggregating basal-like and classical tumours.

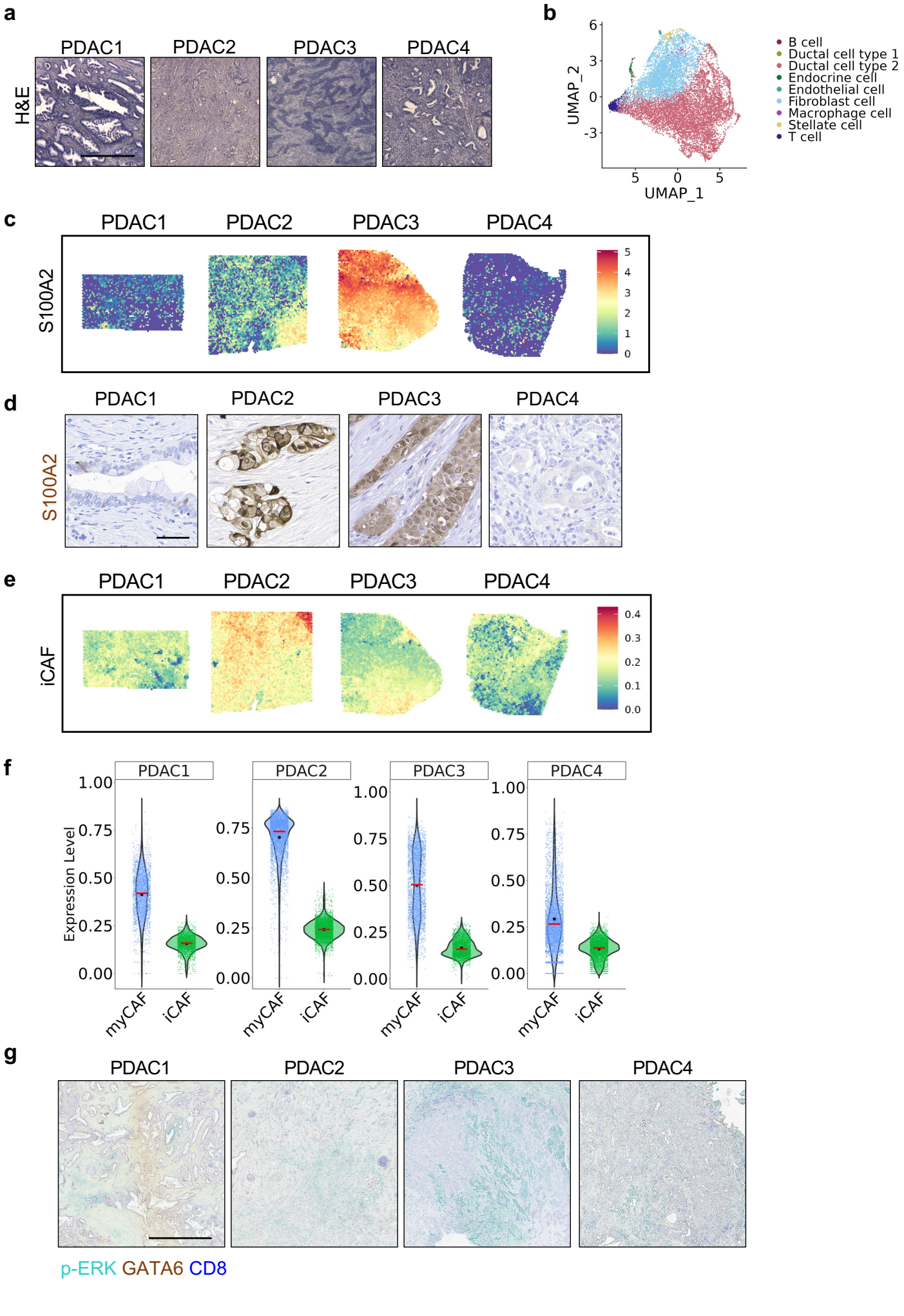
a
PDAC1
PDAC2
PDAC3
PDAC4
H&E
b
UMAP_2
UMAP_1
B cell
Ductal cell type 1
Ductal cell type 2
Endocrine cell
Endothelial cell
Fibroblast cell
Macrophage cell
Stellate cell
T cell
c
S100A2
d
S100A2
e
iCAF
f
Expression Level
myCAF
iCAF
g
p-ERK GATA6 CD8

Supplementary Figure 7. Spatial transcriptomics of human PDAC tissues. a Haematoxylin and Eosin staining of 4 PDAC primary tumours selected for spatial transcriptomics (ST). Scale bar, 1 mm. **b** UMAP plot showing the 9 clusters annotated using on scRNA-seq data from Peng et al.[9] **c** Spatial visualization of S100A2 expression. **d** Immunohistochemical expression of the basal-like marker S100A2 in serial sections of the 4 PDAC tumour tissues subjected to ST. Scale bar, 50 µm. **e** Spatial visualization of the gene module score for the iCAF signature[4] in each section. **f.** Distribution of the gene module scores for the myCAF and the iCAF programs[4] in each section. p values as determined by Wilcoxon test. **g** Low magnification images of the multiplex IHC (p-ERK, GATA6, and CD8) on the four PDAC tumour tissues. Scale bar, 2 mm.

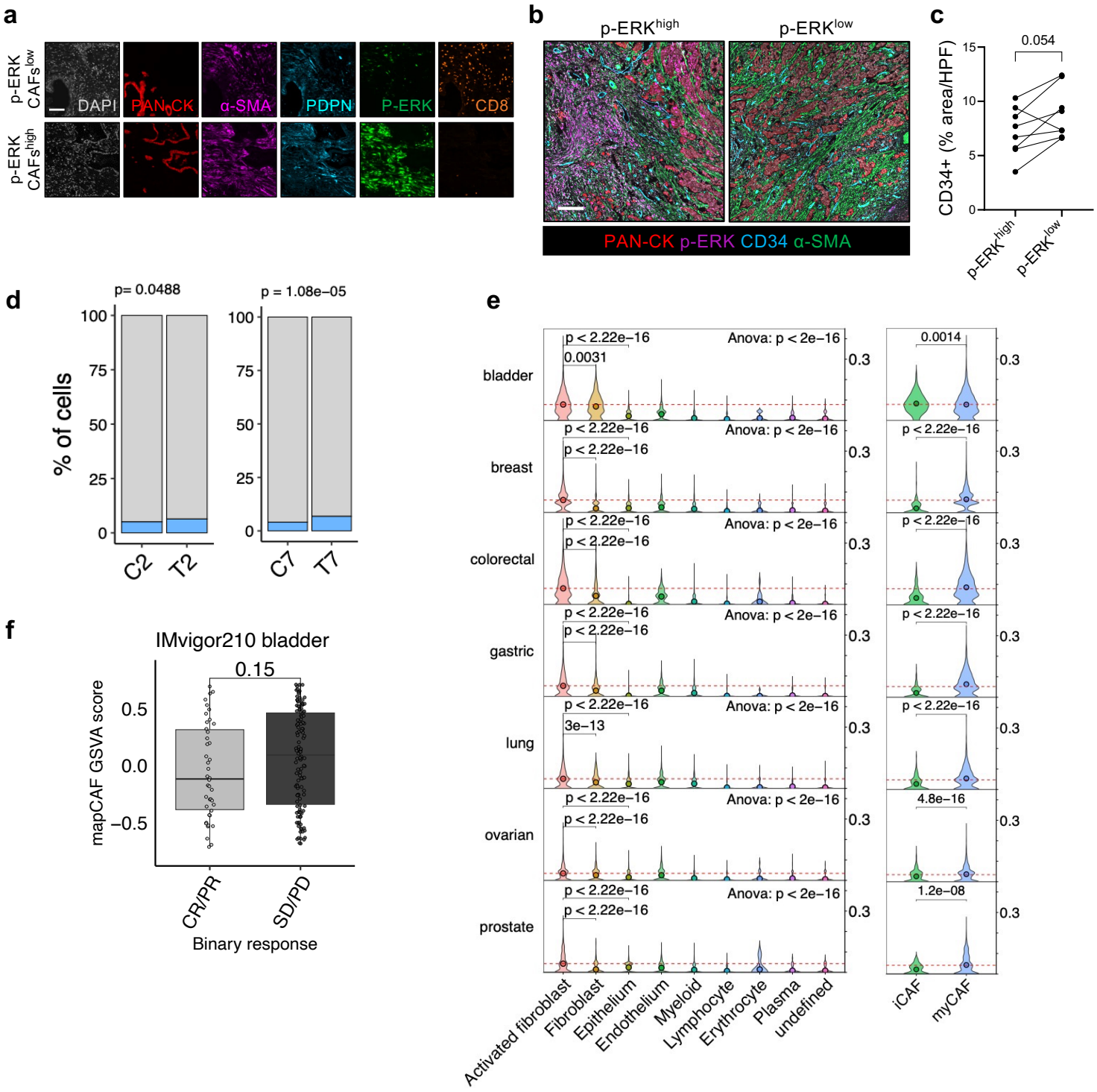
a
p-ERK CAFs low
p-ERK CAFs high
DAPI
PAN-CK
α-SMA
PDPN
P-ERK
CD8
b
p-ERK high
p-ERK low
PAN-CK p-ERK CD34 α-SMA
c
0.054
CD34+ (% area/HPF)
p-ERK high
p-ERK low
d
p= 0.0488
p = 1.08e−05
% of cells
C2
T2
C7
T7
e
bladder
breast
colorectal
gastric
lung
ovarian
prostate
p < 2.22e−16
Anova: p < 2e−16
0.0031
0.0014
3e−13
4.8e−16
1.2e−08
Activated fibroblast
Fibroblast
Epithelium
Endothelium
Myeloid
Lymphocyte
Erythrocyte
Plasma
undefined
iCAF
myCAF
f
IMvigor210 bladder
0.15
mapCAF GSVA score
CR/PR
SD/PD
Binary response

Supplementary Figure 8. The mapCAF phenotype is associated with T cell depleted tumour areas. a. Representative areas from Fig. 7a showing individual fluorescence channels. Scale bar, 100 µm. **b** Representative images of multiplex IF performed on FFPE of human PDAC tissues (n = 8 tissues). The two panels represent different areas within the same tumour displaying either high or low density of p-ERK^{+} CAFs. Scale bar, 200 µm. **c** Paired dot plot showing the quantification of the percentage of CD34^{+} cells in p-ERK^{+} and p-ERK^{-} areas from the same tumour. p values as determined by paired t test (two-sided). **d** Barplot displaying the percentage of T cells (relative to the others non-epithelial populations) from mice treated with either vehicle (C) or MEKi (T) for 2 or 7 days. p values as determined by χ^2 test (two-sided). **e** Violin plots representing the score values for mapCAF signature of cells from different cell type in 7 cancer types from the Luo et al. dataset[13]. Variation of mapCAF signature among all cell types annotated by Anova. Pair-wise comparison between activated fibroblasts and fibroblasts, and between activated fibroblasts and epithelial cells is annotated by Wilcoxon test (two-sided). Comparison between myCAFs and iCAFs on the right is annotated by Wilcoxon test (two-sided) **f** Boxplots showing mapCAF GSVA score in bladder cancers from the IMvigor210 study[14]. Samples (n = 168) are separated by binary drug response. CR, complete response; PR, partial response; SD, stable disease; PD, progressive disease. p values as determined by Wilcoxon test (two-sided). CR/PR: Min -0.71, Max 0.70, Med -0.11, Q1 -0.39, Q3 0.32, IQR 0.70, LW -0.71, UW 0.70. SD/PD: Min -0.70, Max 0.72, Med 0.09, Q1 -0.34, Q3 0.47, IQR 0.81, LW -0.69, UW 0.72.

Supplementary References

1 Moffitt, R. A. *et al.* Virtual microdissection identifies distinct tumor- and stroma-specific subtypes of pancreatic ductal adenocarcinoma. *Nat Genet* **47**, 1168-1178 (2015).

2 Cancer Genome Atlas Research Network. Electronic address, a. a. d. h. e. & Cancer Genome Atlas Research, N. Integrated Genomic Characterization of Pancreatic Ductal Adenocarcinoma. *Cancer Cell* **32**, 185-203 e113 (2017).

3 Subramanian, A. *et al.* Gene set enrichment analysis: a knowledge-based approach for interpreting genome-wide expression profiles. *Proc Natl Acad Sci U S A* **102**, 15545-15550 (2005).

4 Elyada, E. *et al.* Cross-Species Single-Cell Analysis of Pancreatic Ductal Adenocarcinoma Reveals Antigen-Presenting Cancer-Associated Fibroblasts. *Cancer Discov* **9**, 1102-1123 (2019).

5 Jin, S. *et al.* Inference and analysis of cell-cell communication using CellChat. *Nat Commun* **12**, 1088 (2021).

6 Garcia-Alonso, L., Holland, C. H., Ibrahim, M. M., Turei, D. & Saez-Rodriguez, J. Benchmark and integration of resources for the estimation of human transcription factor activities. *Genome Res* **29**, 1363-1375 (2019).

7 Dominguez, C. X. *et al.* Single-Cell RNA Sequencing Reveals Stromal Evolution into LRRC15(+) Myofibroblasts as a Determinant of Patient Response to Cancer Immunotherapy. *Cancer Discov* **10**, 232-253 (2020).

8 Wang, Y. *et al.* Single-cell analysis of pancreatic ductal adenocarcinoma identifies a novel fibroblast subtype associated with poor prognosis but better immunotherapy response. *Cell Discov* **7**, 36 (2021).

9 Peng, J. *et al.* Single-cell RNA-seq highlights intra-tumoral heterogeneity and malignant progression in pancreatic ductal adenocarcinoma. *Cell Res* **29**, 725-738 (2019).

10 Chan-Seng-Yue, M. *et al.* Transcription phenotypes of pancreatic cancer are driven by genomic events during tumor evolution. *Nat Genet* **52**, 231-240 (2020).

11 Steele, N. G. *et al.* Multimodal Mapping of the Tumor and Peripheral Blood Immune Landscape in Human Pancreatic Cancer. *Nat Cancer* **1**, 1097-1112 (2020).

12 Lin, W. *et al.* Single-cell transcriptome analysis of tumor and stromal compartments of pancreatic ductal adenocarcinoma primary tumors and metastatic lesions. *Genome Med* **12**, 80 (2020).

13 Luo, H. *et al.* Pan-cancer single-cell analysis reveals the heterogeneity and plasticity of cancer-associated fibroblasts in the tumor microenvironment. *Nat Commun* **13**, 6619 (2022).

14 Rosenberg, J. E. *et al.* Atezolizumab in patients with locally advanced and metastatic urothelial carcinoma who have progressed following treatment with platinum-based chemotherapy: a single-arm, multicentre, phase 2 trial. *Lancet* **387**, 1909-1920 (2016).

Uncropped western blots

Supplementary Fig 1a

HPAF II

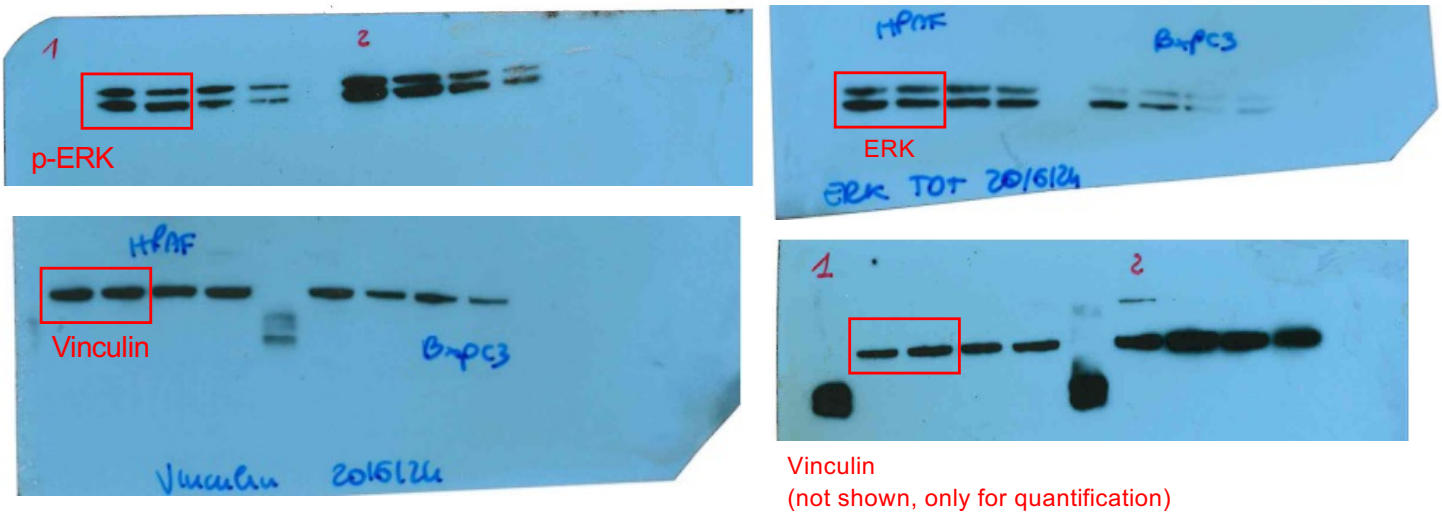

BxPC3

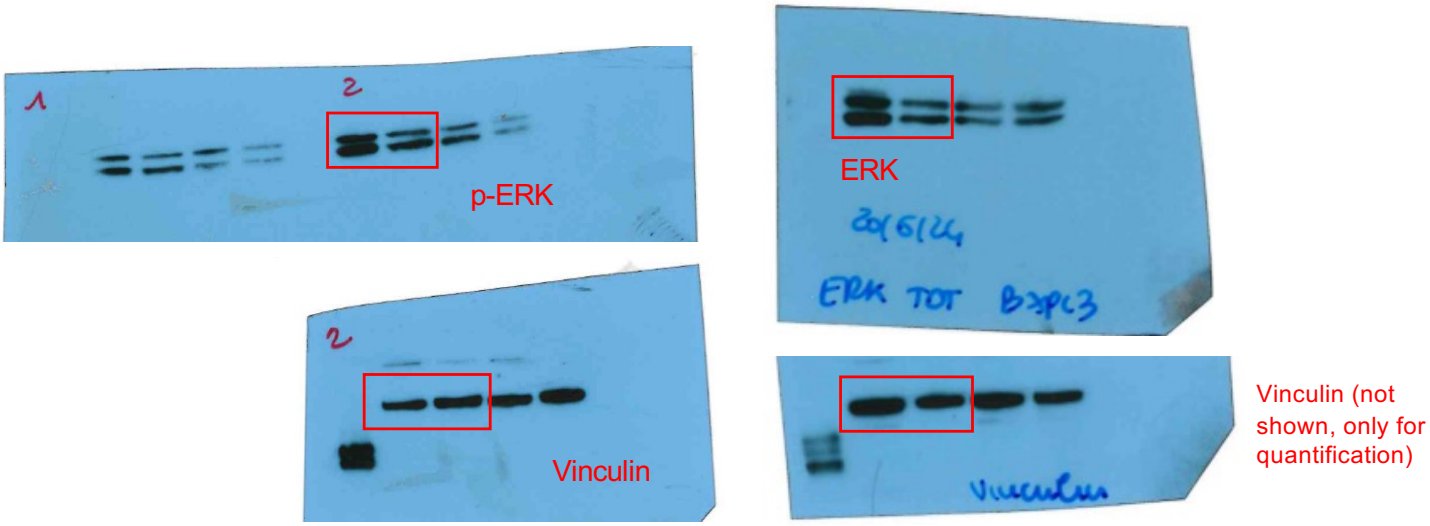

Hs766t

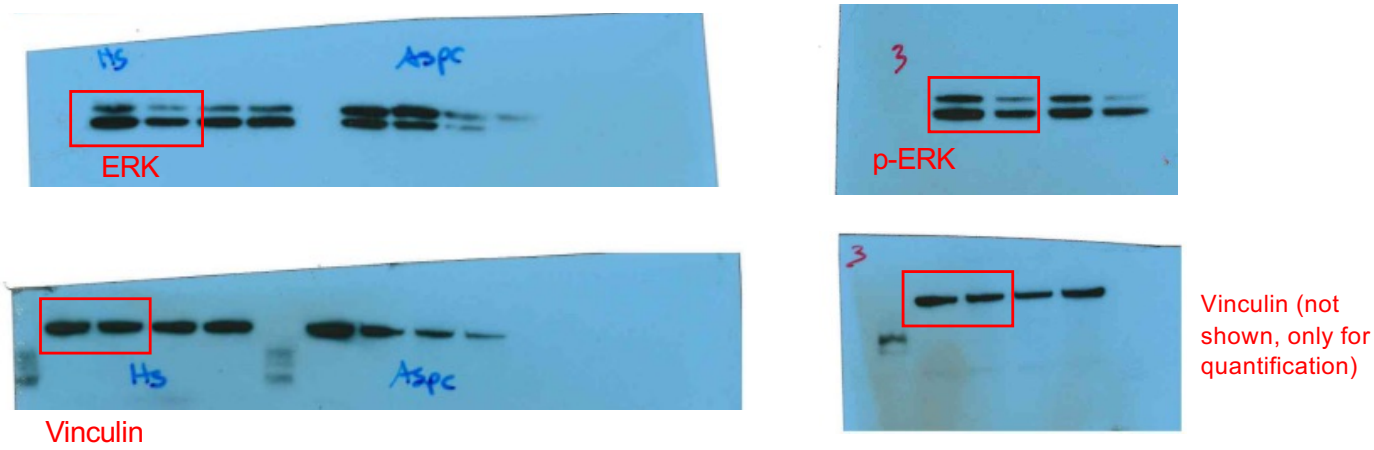

p-ERK: 1:2000 Cell signaling technology #9101

ERK: 1:1000 Cell signaling technology #9102

Vinculin: 1:1000 Cell signaling technology #4650

Supplementary Fig 1a

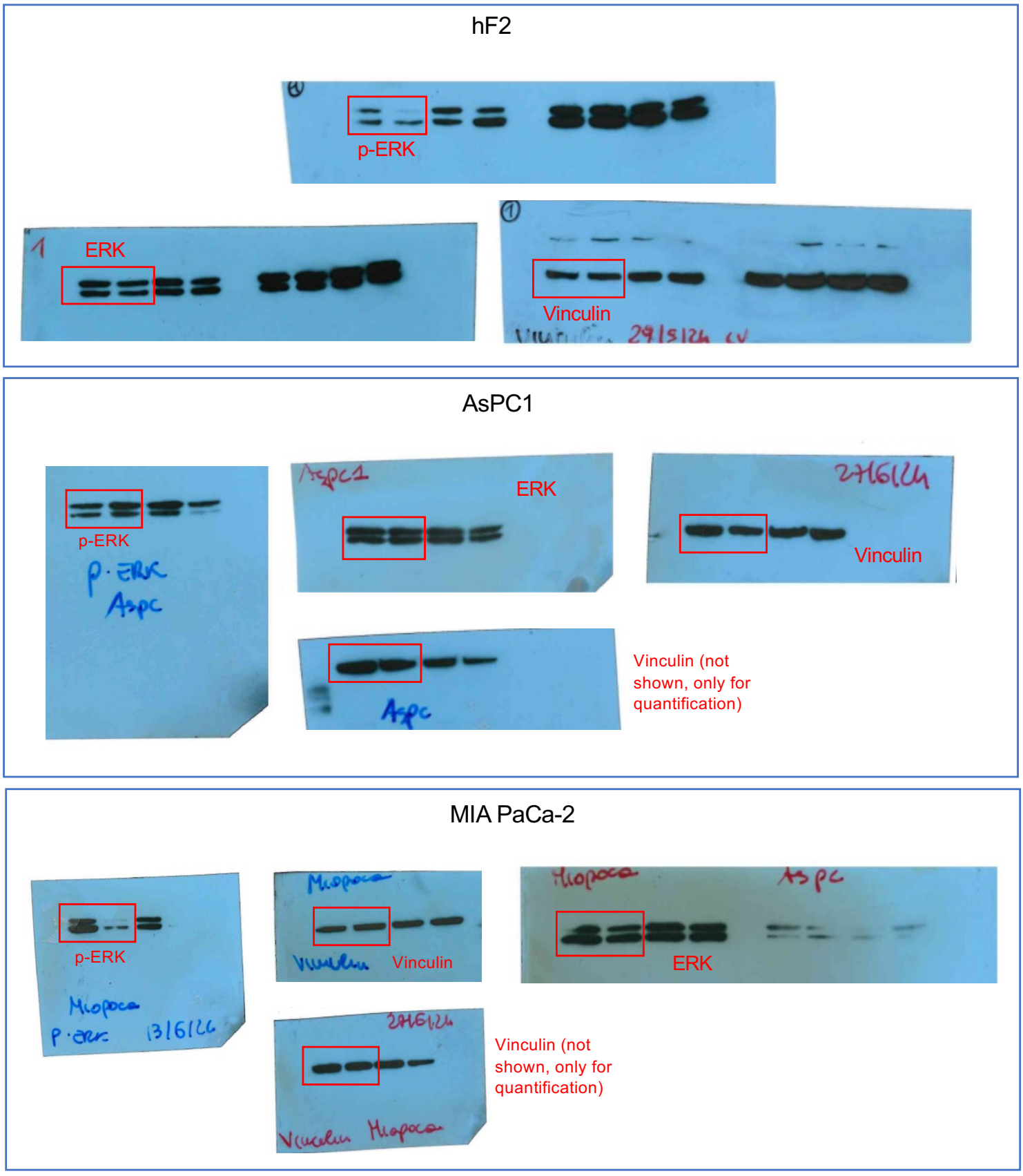

p-ERK: 1:2000 Cell signaling technology #9101

ERK: 1:1000 Cell signaling technology #9102

Vinculin: 1:1000 Cell signaling technology #4650

Supplementary Fig 1a

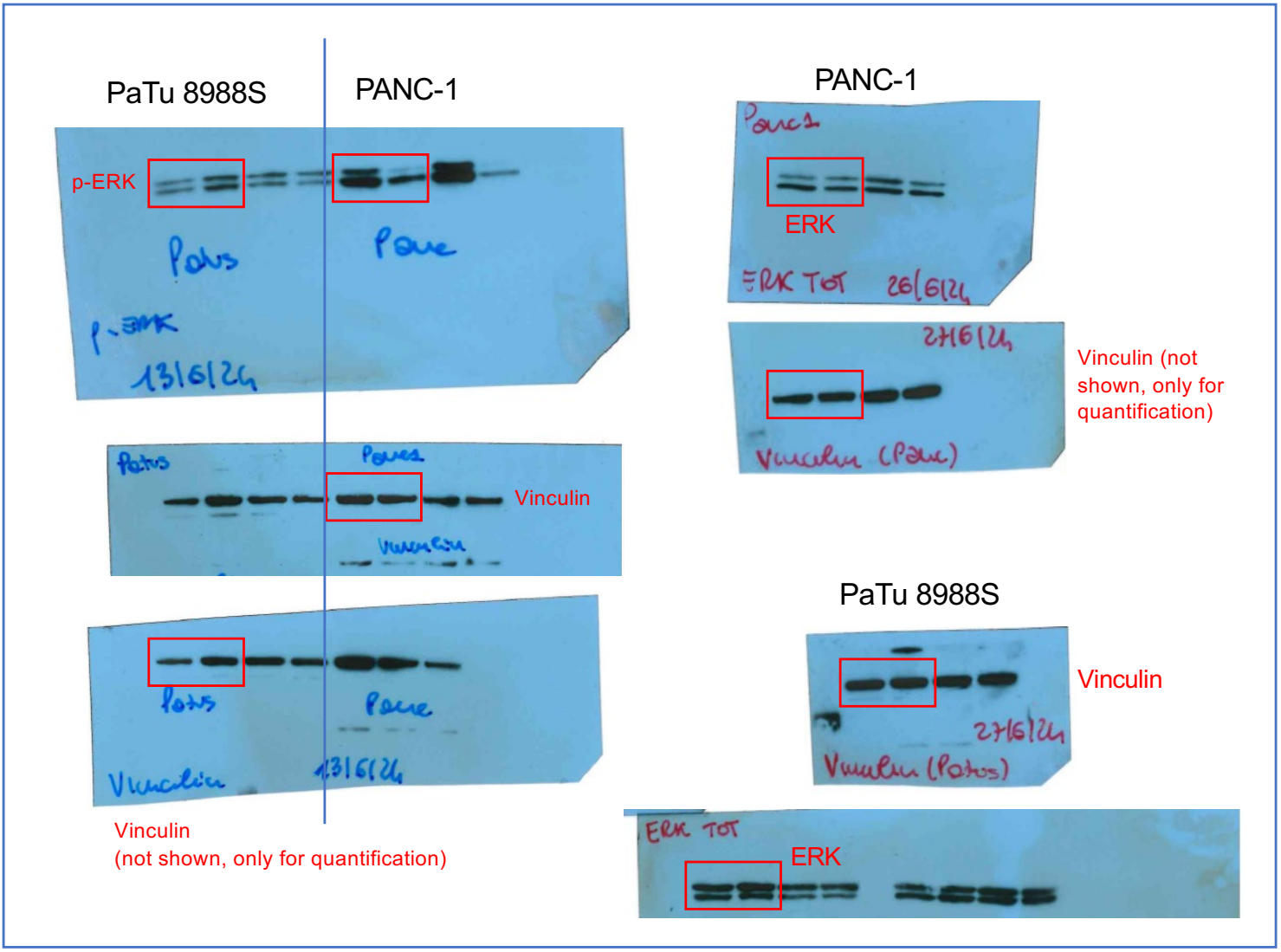

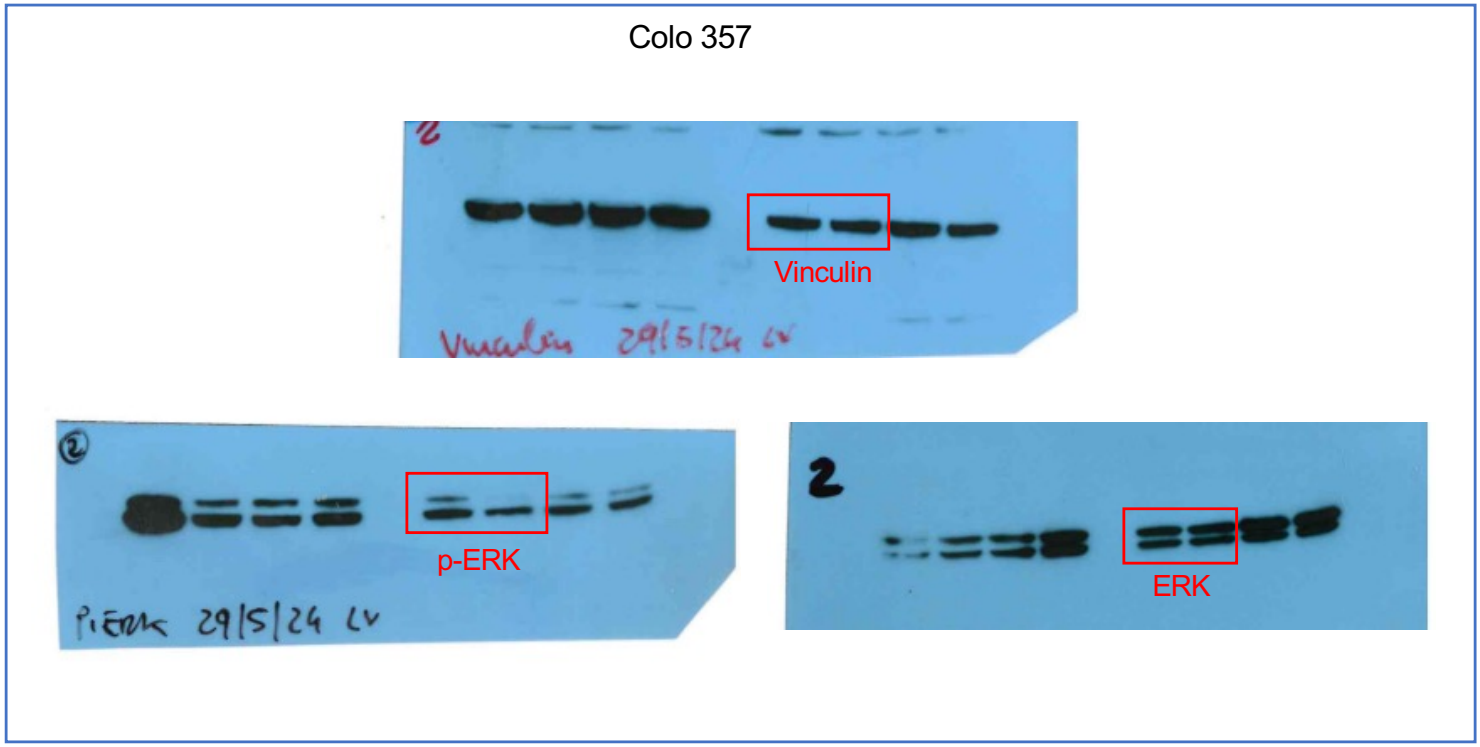

p-ERK: 1:2000 Cell signaling technology #9101

ERK: 1:1000 Cell signaling technology #9102

Vinculin: 1:1000 Cell signaling technology #4650

Supplementary Fig 1a

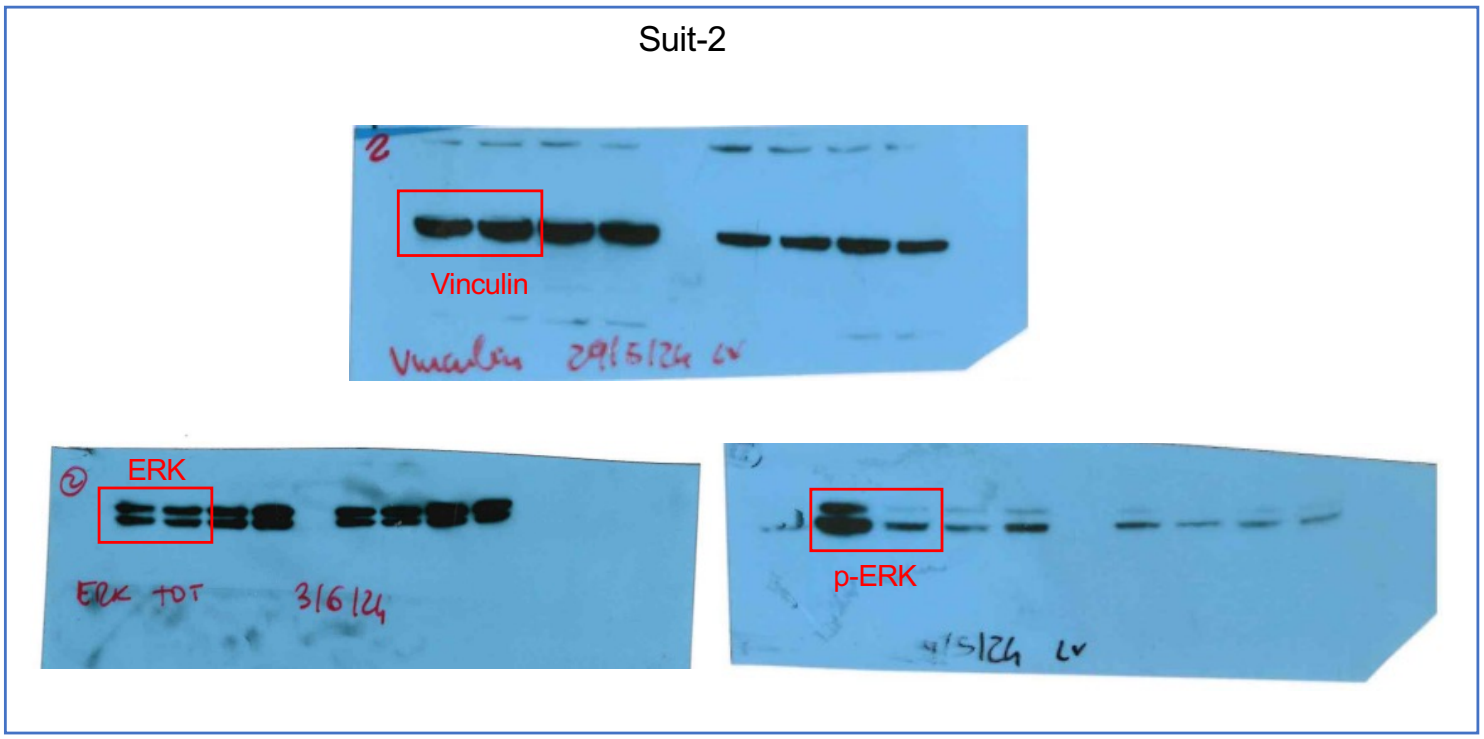

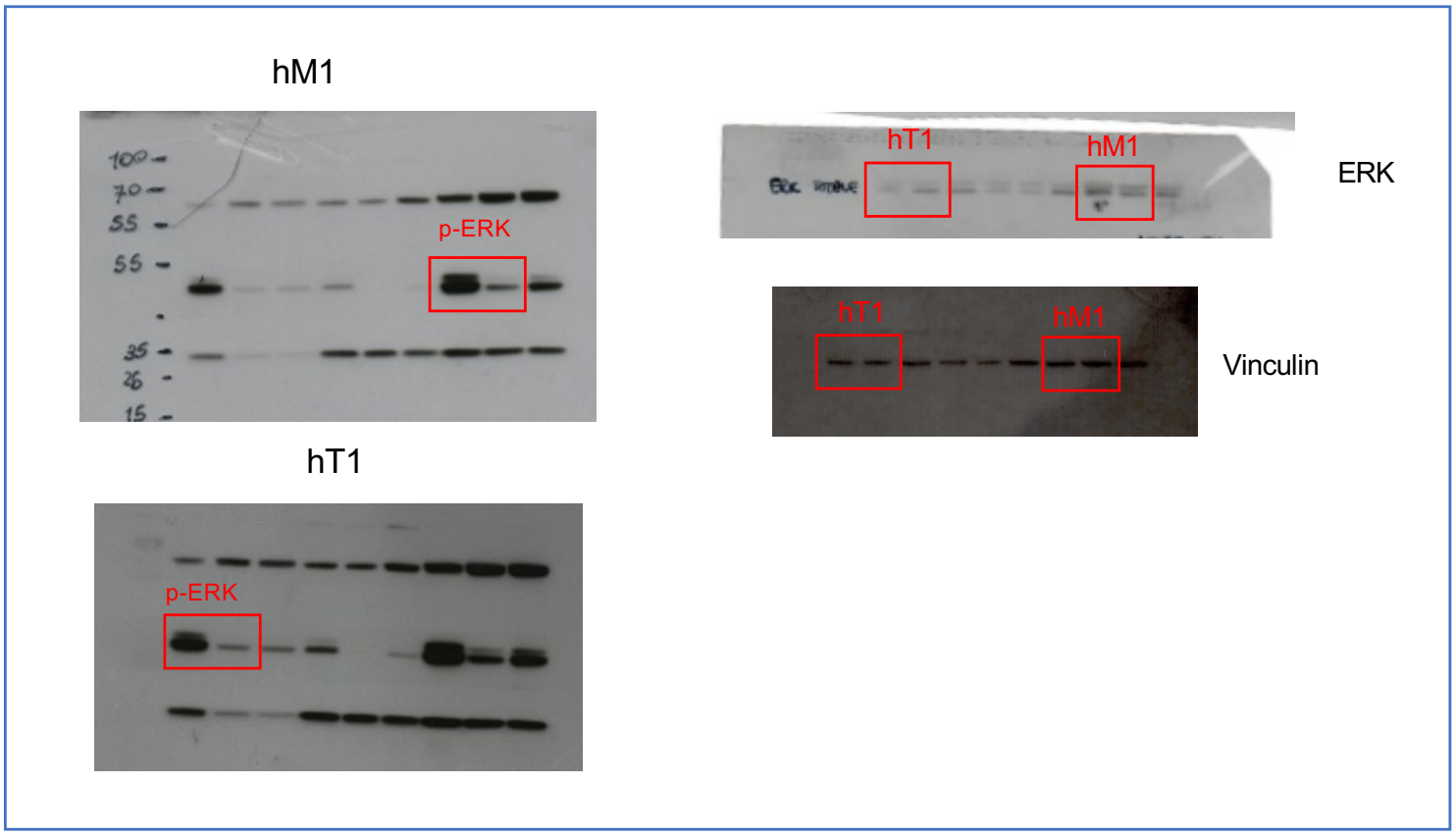

p-ERK: 1:2000 Cell signaling technology #9101

ERK: 1:1000 Cell signaling technology #9102

Vinculin: 1:1000 Cell signaling technology #4650

Supplementary Fig 1h

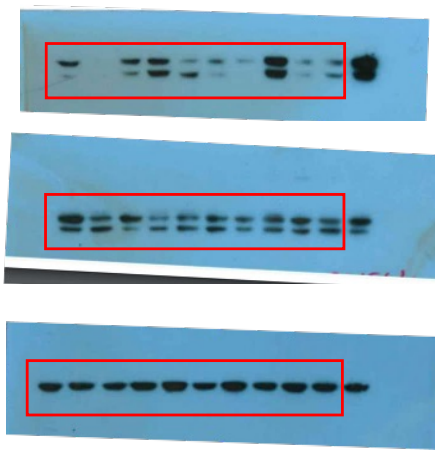

Supplementary Fig 1m

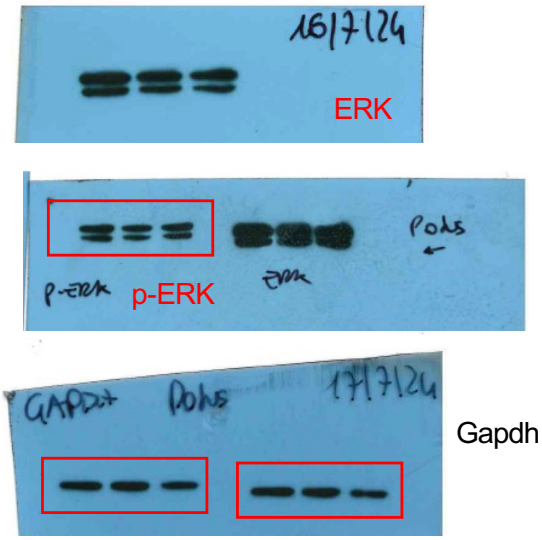

not shown, only
for quantification

p-ERK: 1:2000 Cell signaling technology #9101

ERK: 1:1000 Cell signaling technology #9102

Gapdh: 1:3000 Cell signaling technology #5174

Supplementary Fig 3a

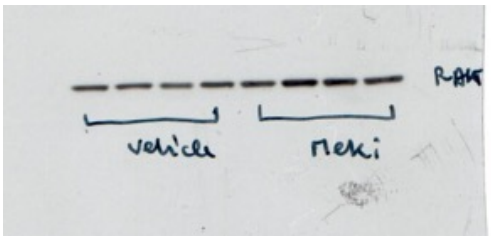

p-AKT: Cell signaling technology #4060

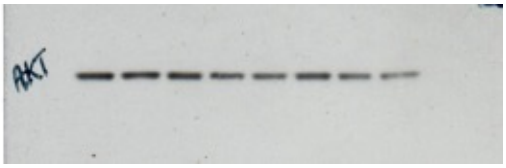

AKT: Cell signaling technology #9272

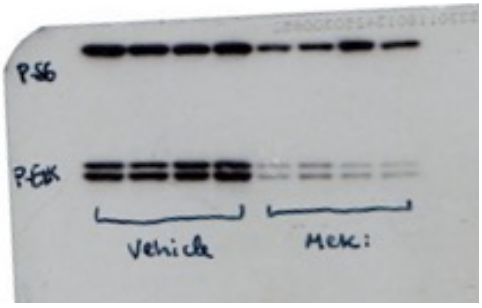

p-S6: Cell signaling technology #D57.2.2E/4858

p-ERK: Cell signaling technology #9101

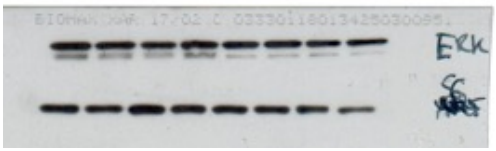

ERK: Cell signaling technology #9102

S6: Cell signaling technology #54D2

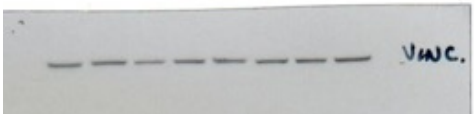

Vinculin: Cell signaling technology #4650

Supplementary Fig 3d

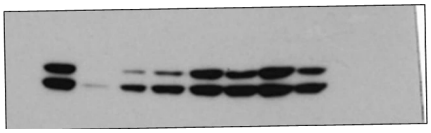

p-ERK: Cell signaling technology #9101

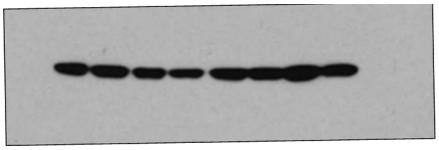

Gapdh: Cell signaling technology #5174